

Wave hindcast studies using SWAN nested in WAVEWATCH III - comparison with measured nearshore buoy data off Karwar, eastern Arabian Sea

M.M.Amrutha¹, V. Sanil Kumar^{1*}, K.G. Sandhya², T.M. Balakrishnan Nair², J.L. Rathod³

¹Ocean Engineering Division, CSIR-National Institute of Oceanography
(Council of Scientific & Industrial Research), Dona Paula, Goa 403004 India

²Information Services and Ocean Sciences Group, Indian National Centre for Ocean Information
Services, Ministry of Earth Sciences, Hyderabad, India

³Post Graduate Department of Marine Biology, Karnatak University, Karwar, India

***Corresponding author:** Tel: 0091 832 2450 327 Fax: 0091 832 2450 602 E-mail: sanil@nio.org

Abstract

Waves in the nearshore waters (~15m water-depth) of eastern Arabian Sea were simulated using SWAN nested in WAVEWATCH III (WW3) for the year 2014. The sensitivity of the numerical wave model WW3 towards different source term (ST) packages was tested. The performance of WW3 was evaluated with the measured deep water buoy data at 15.0000° N, 69.0000° E. Overall, the WW3 wave hindcast results using ST4 physics in deep water show a reasonable match ($r=0.97$ and $SI=0.16$) with the measured significant wave height (H_s). In deep water, a large overestimation (~23.7%) of mean wave period was observed using ST2 compared to ~8.2% using ST4. Komen et al. (1984) whitecapping formulation was found suitable based on the sensitivity studies of SWAN. Simulated H_s using nested SWAN model shows good correlation ($r=0.96$) with the nearshore measured data. During high sea state ($H_s > 2m$), an overestimation (~19.8% for ST2 and ~21.4% for ST4) and during low sea state ($H_s < 1m$), an underestimation (~16.1% for ST2 and ~31.5% for ST4) in mean wave period was observed in the nearshore. WW3 model forced by modified wind field (speed increased by 5%) during June and July resulted in a reduction in underestimation of H_s from 8.6% to 2.2%.

Keywords: Significant wave height, mean wave period, mean wave direction, SWAN, WAVEWATCH III, west coast of India

1. Introduction

Impending waves, which are generated by winds blowing over the sea are the most important environmental force acting on the coastal and offshore structures (Chakrabarti, 2005). Hence, the information on the wave parameters at a location is required in all ocean and coastal engineering projects. The underestimation of wave heights at a location will lead to the failure of the structure and the overestimation will lead to over-design and cost escalation of the project. The wave data covering many years are required for estimation of the design parameters for the coastal and offshore structures, but the measurement of wave parameters over the years at a specific location in the coastal area is a difficult and expensive task. Due to the incompleteness of measured wave parameter over a wide area, satellite observations and wave hindcast models play a key role in wave parameter estimation (Shanas and Sanil Kumar, 2014). Wave hindcasts based on numerical models have become a common tool to get the wave height (Cavaleri et al., 2007) and is currently the only available tool that provides high-resolution (spatial and temporal) long-term wave information in those areas with few or no measurements (Appendini et al., 2014), similar to the north Indian Ocean. Many users depend on now-cast and ocean state forecast for marine related operations (Balakrishnan Nair et al., 2013) and hence, accurate estimation of wave parameters is important. For the wave hindcast, now-cast and forecast, numerical models such as Wave Action Model (WAM) (WAMDI Group, 1988), WAVEWATCH III (WW3) (Tolman, 1989; 1991), MIKE21 Spectral Waves (DHI, 2011), Simulating WAVes Nearshore (SWAN) (Booij et al., 1999) are commonly used (Chawla et al., 2007; Strauss et al., 2007; Remya et al., 2012; Sandhya et al., 2014; Samiksha et al., 2015). WAM and WW3 are more suitable for global and regional scale modelling whereas SWAN is suitable for the nearshore applications. Recently Ocean state forecast has gained much importance and has become a more challenging task, considering the range of wide user community and varied demands. Timely warnings and sea state information are needed by users such as navy, coastguard, fishermen community, ports and harbours, industry and coastal communities. This challenging task is done in India by Earth System Science Organisation-Indian National Centre for Ocean Information Services (ESSO-INCOIS), Hyderabad. They use calibrated, state-of-the-art ocean models for this purpose. Verification of model output is the most important element to gain confidence about the model simulated parameters. It is very important from an operational point of view to quantify the errors associated with a numerical model.

The Arabian Sea is the key region of strong air-sea interaction associated with the Indian summer monsoon (June-September) (Shukla, 1975). Indian summer monsoon shows a wide range of variability on the inter-annual and decadal scale but has its annual regularity (Goswami et al., 2010).

Waves in the eastern Arabian Sea show the seasonal variability due to the seasonality in the winds (Sanil Kumar et al., 2012). Several wave hindcast studies were carried out in the Arabian Sea based on different numerical wave models (Remya et al., 2012; Dora and Sanil Kumar, 2015; Samiksha et al., 2015). The simulated wave parameters based on the MIKE21 model have been validated by comparing with buoy and altimeter data by Remya et al. (2012) and the possible reason for the poorer performance of the model in the Arabian Sea has also been pointed out by them. Nayak et al. (2013) studied the non-linear interaction of distant long-period swells with the local wind-seas in the south-western Bay of Bengal using SWAN coupled with WAM. Sandhya et al. (2014) integrated the two modeling systems viz.; WW3 and SWAN to provide a very high-resolution forecast for Puducherry region. Samiksha et al. (2015) used buoy data to verify the WAM model wave height in the north Indian Ocean for the year 2000-2006 and observed that when the wave heights were relatively small, WAM overestimates the significant wave height (H_s) and underestimates the H_s by 0.5 to 1 m (12 to 25%) during the high sea states ($H_s > 4$ m).

Since the wave models are highly sensitive to wind field variations, the quality of numerical wave hindcast depends to a large extent on the quality and the accuracy of the wind fields (Holthuijsen et al., 1996; Moeini et al., 2012). Study of Kumar et al. (2000), for the Indian Ocean, reported that the wave height and wave period estimation are dependent on the precision of the wind field used to force the model. In most of the wave hindcast studies, the difference between model output and measured parameters is due to the inaccurate wind field. A 10% error in the estimate of surface wind speed can lead to a 10-20% error in the H_s (Cavaleri, 1994). Thus, the selection of appropriate wind source is a vital step in the wave modeling. Moeini et al. (2010) used SWAN model for wave hindcasting in the Persian Gulf using European Centre for Medium-Range Weather Forecasts (ECMWF) winds and measured wind data. The wind field in the equatorial region is observed to be inaccurate in the reanalysis data (Ji and Smith, 1995; Kelly et al., 1999; Putman et al., 2000; Kumar et al., 2012). The *BIAS*, correlation coefficient, root mean square error (*RMSE*) and scatter index (*SI* in %) between the measured and the ECMWF wind data for the tropical Indian Ocean are 0.8 m/s, 0.57, 2.6 m/s and 52.5, respectively (Harikumar et al., 2013). The earlier studies have shown that bathymetry is also an important factor (Chawla, 2007; Brown and Wolf, 2009). Hence, both bathymetry and wind field are sensitive components for the numerical wave model.

At any given time, the eastern Arabian Sea contains swells from the south Indian Ocean and wind-seas originating from a wide variety of wind-generation events (Glejin et al., 2013; Anoop et al., 2015; Anoop et al., 2016). The studies in the eastern Arabian Sea indicate that wave spectrum is predominantly multi-peaked due to the coexistence of swells and wind-seas (Sanil Kumar et al.,

2003). The earlier studies (Remya et al., 2012; Sandhya et al., 2014) in the north Indian Ocean show that the wave hindcast results in the shallow water deviates from the measured value at locations where wind-seas are superimposed on swells. Hence, we have examined the sensitivity of the numerical model SWAN nested in WW3 for a location in the eastern Arabian Sea where wind-seas and swells coexist.

2. Materials and methods

2.1 Study location

The location selected for the study is off Karwar in eastern Arabian Sea (Fig. 1). The location is exposed to deep-water swells from the south Indian Ocean and the distance of the location from the west coast of Indian mainland is 5 km. Waves at this location during the non-monsoon period were swells superimposed on wind-sea and during the monsoon predominance of swells was observed (Dora and Sanil Kumar, 2015). Hence, multi-peaked spectrum frequently occurred during January to April, and the single-peaked spectrum was found mainly during the monsoon period (Dora and Sanil Kumar, 2015). The study location experiences rough sea state ($H_s > 1.5$ m) during the monsoon period, and is relatively calm ($H_s < 1.5$ m) during rest of the year. Further, over an annual cycle, the sea surface was composed of 36% wind-seas and 64% swells (Dora and Sanil Kumar, 2015). The tides of the study area are predominantly semi-diurnal and mixed with an average tidal range of 1.58 m during the spring tide and 0.72 m during the neap tide (ITT, 2014).

2.2 Wave model

We used the WW3 version 4.18 developed at NOAA/NCEP (National Centres for Environmental Prediction) and SWAN 41.01 developed at Delft University of Technology for the wave hindcast study. WW3 is one of the effective tools for global and regional scale wave modelling studies and has been implemented in different parts of the world for studying the wave spectral evolution, air-sea interactions and non-linear wave-wave interactions in deep water (Tolman, 1989; 1991). SWAN is developed for estimation of wave parameters in coastal regions (Booij et al., 1999; Ris et al., 1999). SWAN, which is computationally less efficient in the deep water, uses implicit scheme, whereas WW3 uses explicit and semi-implicit scheme for source term. So the nesting of SWAN in WW3 is a convenient option for better simulation of wave parameter in nearshore areas. The model physics and other details of WW3 are described in several works (e.g. Tolman, 1991; 2008) and that for SWAN by Booij et al. (1999), Ris et al. (1999) and Chris Bunney (2011).

Two model grids were used for the present study. The coarse grid of WW3 ranges from 70° S to 35° N and from 20° E to 112° E in 210 x 184 equidistant grids with a resolution of 0.5° (Fig. 1). The

model domain was finalised after checking the sensitivity connected to the selection of domain for the wave modelling. Considering only the area above 40° S for the model domain resulted in 17% error in the simulated H_s in deep water and for the area above 20° S resulted in 20% error whereas restricting the model domain to be the area above equator resulted in 25% error in the H_s . The fine grid used in the SWAN model has a domain from 13.50° N to 16.00° N and 72.75° E to 74.74° E in 250 x 199 equidistant grids with a resolution of 0.01°. Nesting of these models enables to simulate remotely generated swells in the South Indian Ocean propagating into the eastern Arabian Sea, and to reduce expensive high-resolution grids for the entire domain. The 1-minute resolution bathymetry data from ETOPO1 (Amante and Eakins, 2009) available from the National Geophysical Data Center was used in WW3 simulations while the digitised data from national hydrographic chart No. 2008 was used in SWAN simulations to take care of the variations in bathymetry in nearshore areas. The nested domain for SWAN model encompasses the coastal area off Karwar. The wind data used in the study is ERA-Interim (Dee et al., 2011) from ECMWF with a temporal resolution of 6-h and spatial resolution of 0.5° and 0.25° respectively for WW3 and SWAN. Wave frequencies were discretized from 0.04 to 1 Hz over 25 bins on a logarithmic scale; 36 bins of 10° each were taken for direction. WW3 was tested with both the source term packages ST2 and ST4 physics and the obtained two-dimensional energy density spectra were used as the boundary conditions for nearshore model SWAN. Boundary conditions from WW3 with different physics options were given to the nested SWAN and the results were compared. The processes activated in SWAN simulations include depth-induced wave breaking (Hasselmann et al., 1973), bottom friction, wind-wave growth, whitecapping, quadruplet and triad interactions (Eldeberky, 1996). WW3 uses four time steps: global time step, the spatial time step, the directional time step, and the source term time step, in seconds. The spatial time step Δt_{xy} is determined first, since it is the time step for spatial propagation, and must satisfy the Courant-Friedrichs-Levy (CFL) criteria. This is determined by the grid's resolution, the maximum latitude in the grid, and the first frequency. $\Delta t_{xy} = \frac{\Delta x}{C_g} = 123766 * \Delta x * \cos d(\max lat) * f$ (Spindler and Tolman, 2008). The global time step Δt_g is set to be 2 or 3 times Δt_{xy} approximately. Once the Δt_g is determined, the directional time step (Δt_k) is set to $0.5 * \Delta t_g$. In the present study, the source time step is set as 30 s, which is the generally used value.

2.3 Measured data

Measured wave data during January-December 2014 obtained from the Datawell directional waverider buoy (0.9 m diameter) equipped with a three-component (x, y, z) acceleration sensor and a

two-component (x, y) tilt sensor was used for comparison of the wave hindcast results at nearshore (15 m water depth) (geographic position 14.8217° N and 74.0524° E). The buoy reports frequency spectra and directional moments in the frequency range 0.025 to 0.58 Hz every half hour based on 30-minute long records of x, y and z-displacements. The frequency bandwidths of the spectra are 0.005 Hz below 0.1 Hz and 0.01 Hz above 0.1 Hz. The details of the wave data analysis are presented in Sanil Kumar et al. (2014).

The measured wave data collected in the AS using a moored Seatex buoy (Oceanor, Norway) (Premkumar et al., 2000) at 3000 m water depth in AD2 location (15.0000° N; 69.0000° E) during June-December 2009 was used for the comparison of the hindcast H_s in deep water. The heave data was recorded at 2 Hz interval for 17 minutes duration and from the recorded heave data, the wave spectrum was obtained through fast Fourier Transform and the H_s was estimated from the zeroth spectral moment (m_0) as $H_s = 4 \sqrt{m_0}$.

Model results are statistically compared with measured buoy data using Pearson's linear correlation coefficient (r), *BIAS*, root-mean-square error (*RMSE*), and scatter index (*SI*).

$$BIAS = \frac{1}{N} \sum_{i=1}^N (A_i - B_i) \quad (1)$$

$$RMSE = \sqrt{\frac{1}{N} \sum_{i=1}^N (A_i - B_i)^2} \quad (2)$$

$$SI = \frac{RMSE}{\bar{B}} \quad (3)$$

$$r = \frac{\sum_{i=1}^N [(A_i - \bar{A})(B_i - \bar{B})]}{\sqrt{\sum_{i=1}^N [(A_i - \bar{A})^2 (B_i - \bar{B})^2]}} \quad (4)$$

Where A_i represents the parameter based on the numerical model, B_i represents the measured parameter, N is the number of data points, and the overbar represents the mean value.

3. Results and discussion

To evaluate the performance of WW3, simulated values of H_s and mean wave period (T_{m01}) were compared with the measured values at a deep water location. Several test simulations were carried out using the physics packages ST2 and ST4 in WW3. The results show that ST4 simulation results

in an underestimation of 8.28% for H_s and an overestimation of 8.2% for T_{m01} , while ST2 simulation results in an overestimation of 10.52% for H_s and an overestimation of 23.7% in T_{m01} (Fig. 2). At this location, H_s was above 3 m during June and July with the maximum measured value of 6.5 m, whereas the maximum simulated H_s was 5.5 m (Fig. 2). A comparison of the time series of H_s from the WW3 model and measurement (Fig. 2a) suggests that they give comparable results except during high waves. It is observed that the simulation of high waves with H_s more than 4 m was underestimated ($\sim 9.87\%$) by the numerical model. The scatter plots for different wave parameters are also presented in Fig. 2 and the comparison statistics for wave parameters were calculated and presented in Table 1. Since the high waves ($H_s > 4$ m) were underestimated by WW3, the simulations were repeated by increasing the wind speed by a factor of 5 and 10% during June and July when the high waves persist. It was observed that on increasing the ERA-Interim wind speed by 5% during June and July, the H_s underestimation reduced from 8.57% to 2.22%. Increasing the ERA-Interim wind speed by 10% during June and July, the H_s overestimated by 4.41%.

SWAN simulation was carried out with the third generation non-stationary mode at 30-minute time step. Many simulations were carried out for choosing appropriate physics for the SWAN model also. An example showing the estimated H_s based on the simulations with different formulations in SWAN during the monsoon period is presented in Fig. 3. Three different whitecapping formulations (i.e., Komen et al., Janssen, and Westhuysen) were also tested. The statistical parameters for the respective simulations are given in Table 2. Komen et al. (1984) whitecapping formulation was found suitable based on the sensitivity studies of SWAN. The quadruplet and triad wave-wave interactions were also activated. The quadruplets can be integrated by four different numerical procedures; quad 1 (semi-implicit computation of the nonlinear transfer with DIA per sweep), quad 2 (fully explicit computation of the nonlinear transfer with DIA per sweep), quad 3 (fully explicit computation of the nonlinear transfer with DIA per iteration), quad 8 (fully explicit computation of the nonlinear transfer with DIA per iteration, but neighbouring interactions are interpolated in piecewise constant manner). All these options were tested and found that the variations in the estimated H_s were negligible. Hence, the default quad 2 was used in the study. Other parameters found suitable for the study location were; JONSWAP formulation with γ 0.038 $m^2 s^{-3}$ for bottom friction and Battjes & Janssen model for depth-induced wave breaking with values of 1 for α and 0.73 for γ . The H_s , T_{m02} and mean wave direction (Dir) from nested SWAN model were extracted for the study area for the year 2014.

To evaluate nested model's performance, a detailed validation study is performed by comparing model-simulated wave parameters with corresponding buoy observations in the nearshore for one

year period covering different seasons. Fig. 4 represents the comparison between measured and model-simulated wave parameters off Karwar during 2014. It is observed that for certain periods, the hindcast H_s and measured data are in good agreement (Fig. 4). Simulation results showed that 1.3% of the waves have H_s more than 3 m, whereas the observations show that 2.5% of the waves belong to this category. Dir and T_{m02} are showing the variations similar to the measured values, but with larger deviations (Figs. 5 and 6). During high sea state ($H_s > 2\text{m}$), an overestimation ($\sim 19.8\%$ for ST2 and $\sim 21.4\%$ for ST4) and during low sea state ($H_s < 1.0\text{m}$), an underestimation ($\sim 16.1\%$ for ST2 and $\sim 31.5\%$ for ST4) in mean wave period was observed in the nearshore based on the nested model. The measured data shows that 88% of the time waves were from the sector between south and west, whereas the model results show that 91% of the time they were from the same sector. The statistics of each wave parameter for comparing the model efficiency are calculated and are presented in Table 3.

Since there is a large seasonal variation in wave parameters of the study area (Dora and Sanil Kumar, 2015), we separated the data for different seasons to know the seasonal bias during; pre-monsoon (FMAM), monsoon (JJAS) and post-monsoon (ONDJ) period and the scatter plot between measured and hindcast data off Karwar are presented (Fig. 7). The comparison statistics for wave parameter were calculated for pre-monsoon, monsoon, post-monsoon separately and presented in Table 3. During monsoon period, the 6-h measured H_s range from 0.60 to 4.02 m with a mean value of 1.87 m and standard deviation (SD) of 0.69 m, whereas the simulated values range from 0.76 to 3.56 m with a mean value of 1.90 m and SD of 0.61 m. For the pre-monsoon season, the measured H_s ranges from 0.35 m to 1.40 m with mean value of 0.76 m and SD of 0.18 m, and that of the model were 0.50 m to 1.23 m with mean value of 0.78 m and SD of 0.16 m. In the case of post-monsoon, 0.29 m to 1.55 m and 0.47 m to 1.26 m were the ranges of measured and modeled H_s with mean values of 0.61 m and 0.71 m respectively. The SD during the post-monsoon was 0.21 and 0.14 m for measured and modelled H_s . In the North Indian Ocean, higher SD was observed during monsoon compared to other seasons (Anoop et al., 2015). The study shows that the seasonal mean H_s values obtained from the nested model was close to the measured values. Similarly the difference between the annual mean value of measured (~ 1.08 m) and modelled (~ 1.13 m) H_s was small. It can be seen that for monsoon period, the scatter index is minimum, and correlation is high compared to pre and post-monsoon periods. One possible reason for this is; during the monsoon period, the swells are the major forcing, whereas, during the pre-monsoon, sea breeze has an impact on the diurnal cycle of the sea state of the eastern Arabian Sea (Neetu et al., 2006; Glejin et al., 2013). The large scale wind data used in the

study may not represent the coastal land/sea breeze effect and hence resulted in large deviations in wave period during the pre and post-monsoon periods.

Similarly, the comparison between the model-simulated parameters using ST4 physics and measured ones was carried out. The statistical parameters were calculated for the year 2014 and are given in Table 3. The simulated H_s were overestimated (11.2%) by ST2, whereas it was underestimated (0.48%) by ST4. The T_{m02} and peak wave period (T_p) were underestimated using both ST2 and ST4 during the pre- and post-monsoon seasons (Table 3). In the case of T_{m02} , ST4 simulation is more acceptable than ST2. The scatter plot for different seasons using ST4 is shown in Fig. 8. Moeini et al. (2010) applied the ECMWF and the measured wind data for wave modeling in the Persian Gulf using the SWAN model and observed overestimation of the low wave heights by model due to the overestimation of low wind speeds and underestimation of the high waves due to the high wind speed underestimation by ECMWF. The ERA-Interim wind data used in the study at the deep water point in the Arabian Sea is compared with the buoy measured wind data and is presented in Fig. 9. Since the measured wind data was at ~ 3 m from the mean sea level (MSL), the wind data was converted to 10 m elevation with respect to MSL based on the wind profile power law (Roland, 1988) as per $U_Z = U_R * (Z/R)^\alpha$, where U_Z is the wind speed at Z elevation, U_R is the wind speed measured at R elevation, and α is the power law exponent and is equal to 1/7. The discrepancy between ERA-Interim and measured wind field are shown in Fig. 9. Winds of ERA-Interim are averaged for $0.75^\circ \times 0.75^\circ$, whereas the measured data is at a point. Another reason for the error in the simulated wave parameters is due to the fact that the model output is at 20 m water depth, whereas the measured parameters are at 15 m. Along the west coast of India, Aboobacker et al. (2013) reported that between 25 and 15 m water depth off Goa and between 35 and 15 m depth off Ratnagiri during the pre-monsoon period, the reduction in significant wave height is less than 10%. Amrutha et al. (2015) reported that during 18 April - 18 August, the H_s at 9 m water depth is approximately 15% less than the value at 30 m.

During monsoon period, the mean wave direction is well simulated by the model mainly due to accurate prediction of south-westerly and westerly winds. But during the non-monsoon period, the numerical model fails to produce the north-west wind-sea (Fig. 7). Along the eastern Arabian Sea, during the non-monsoon period, coexistence of wind-sea and swell are observed with predominance of swells (Glejin et al., 2013; Sanil Kumar et al., 2014; Dora and Sanil Kumar, 2015) and hence, measured data shows two peaks; south-west swells and the north-west wind-sea, but the simulated data shows mainly the south-west swells. The wind rose diagram for the year 2011 shows that winds were from the sector between north and west during 33% of the time in the measured data, whereas it

was 27% in the ERA-Interim data. Both the data sets shows 30% of the winds from the sector between south and west (Fig. 9). Hence, the numerical model could not produce the north-west wind-sea. This also resulted in low correlation between the measured and model simulated T_p .

4. Conclusion

The significant wave height and mean wave period obtained from the WW3 model were compared at a deep water point with measured buoy data. In the deep water, a large overestimation (~23.7%) of mean wave period was observed using ST2 compared to ~8.2 % using ST4. The wave parameters (significant wave height, mean wave period and mean wave direction) were simulated in the nearshore off Karwar using SWAN nested with WW3 and compared the results with the measured data at 15 m water depth. The simulated results for the year 2014 shows that the nested model can estimate the significant wave height (H_s) comparable to the observed data. The comparison result of the rest of the parameters is not as accurate as H_s . The model simulates H_s to a good level of accuracy using both ST2 and ST4 physics of WW3. In the case of mean wave period, ST4 simulation is more acceptable than ST2. During the monsoon season, the scatter index of estimated wave parameters is minimum, and correlation is high compared to the non-monsoon period since during the monsoon period the swells are dominated. WW3 model forced by modified wind field during June and July resulted in the reduction of underestimation of significant wave height from 8.6% to 2.2%. From the figures and statistics presented in this article, it is concluded that the results are reasonably good. Thus, the various model parameters, model setup and bathymetry identified for the study area can be used in the near-shore wave simulation for improving the ocean state forecast given out by operational agencies.

Acknowledgments

The authors gratefully acknowledge the financial support given by the Earth System Science Organization, Ministry of Earth Sciences, Government of India to conduct part of this research. The Director of the CSIR-National Institute of Oceanography, Goa and the Director of the INCOIS, Hyderabad provided encouragement in carrying out the study. We thank Mr. Arun Nherakkol, Scientist, INCOIS, Hyderabad and Mr. Jai Singh, Technical Assistant at CSIR-NIO for assistance during the data collection. We also thank Mr Seemanth M (ISRO) and Mr. Dora G. U., Research Scholar, NIO for their valuable support. This is NIO contribution ----and INCOIS contribution

Reference

- Aboobacker, V.M., Vethamony, P., Samiksha, S.V., Rashmi, R., and Jyoti, K., 2013. Wave transformation and attenuation along the west coast of India: Measurements and numerical simulations. *Coastal Engineering J.* 55(01), 1350001–1350022.
- Amante, C., Eakins, B.W., 2009. ETOPO1 1 arc-minute global relief model: Procedures, data sources and analysis. NOAA Tech. Memo. NESDIS NGDC-24, 19 pp.
- Amrutha, M.M., Sanil Kumar, V. and Singh, J., 2016. Changes in nearshore waves during the active sea/land breeze period off Vengurla, central west coast of India, *Annales Geophysicae* 34, 215-226, doi:10.5194/angeo-34-215-2016.
- Anoop, T.R., Sanil Kumar, V., Shanas, P.R., Johnson, G., 2015. Surface wave climatology and its variability in the North Indian Ocean based on ERA-Interim reanalysis, *J. Atmospheric and Oceanic Technology* 32, 1372-1385. doi.:10.1175/JTECH-D-14-00212.1
- Anoop, T.R., Sanil Kumar, V., Shanas, P.R., Johnson, G., Amrutha, M.M., 2016. Indian Ocean Dipole modulated wave climate of eastern Arabian Sea, *Ocean Science*, doi:10.5194/osd-12-2473-2015.
- Appendini, C., Torres-Freyermuth, A., Salles, P., Lopez, J., Mendoza, E.T., 2014. Wave climate and trends for the Gulf of Mexico: A 30-yr wave hindcast. *J. Climate* 27, 1619-1632. doi: 10.1175/JCLI-D-13-00206.1.
- Balakrishnan Nair, T.M., Sirisha, P., Sandhya, K.G., Srinivas, K., Sanil Kumar, V., Sabique, L., Nherakkol, A., Prasad, B.K., Kumari, C.R., Jeyakumar, Kaviyazhahu, K., Kumar, M.R., Harikumar, R., Sheno, S.S.C., Nayak, S., 2013. Performance of the Ocean State Forecast system at Indian National Centre for Ocean Information Services. *Current Science India* 105(2), 175-181.
- Booij, N., Ris, R.C., Holthuijsen, L.H., 1999. A third-generation wave model for coastal regions 1. Model description and validation. *J. Geophysical Res.* 104 (4), 7649- 7666.
- Brown, Jennifer M., and Judith Wolf., 2009. Coupled wave and surge modelling for the eastern Irish sea and implications for model wind-stress. *Continental shelf Res.* 29(10), 1329-1342.
- Cavaleri, L., 1994. Wave models and input wind. *Wave Dynamics and Modelling of Ocean Waves*, G. J. Komen et al., Eds., Cambridge University Press, 259–378.
- Cavaleri, L., Alves, J.-H.G.M., Ardhuin, F., Babanin, A., Banner, M., Belibassakis, K., Benoit, M., Donelan, M., Groeneweg, J., Herbers, T.H.C., et al., 2007. Wave modeling: the state of the art. *Prog. Oceanogr.* 75, 603–674.
- Chakrabarti, S.K., 2005. *Handbook of Offshore Engineering, Vol-1, Ocean Engineering Series*, Elsevier, 661 pp.
- Chawla, A., 2007. *Global Bathymetry Validation Study. MMAB Contribution No. 253.*
- Chawla, A., Cao, D., Gerald, V., Spindler, T., Tolman, H., 2007. Operational implementation of a multi-grid wave forecasting system. 10th International workshop on wave hindcasting and forecasting, 1-12, Oahu, Hawaii.
- Chris, Bunney, 2011. *A High Resolution SWAN Model Assessment: North Norfolk to Humber. Met Office Forecasting Research Technical Report 557 .*
- Deanna, M.S., Tolman, H. 2008. Example of WAVE WATCH III for the NE Pacific. Technical Note 259. National Oceanic and Atmospheric Administration National Weather Service National Centers for Environmental Prediction 5200 Auth Road Room 207 Camp Springs, MD 20746, USA.

- Dee, D.P., et al., 2011. The ERA-Interim reanalysis: Configuration and performance of the data assimilation system. *Q. J. R. Meteorolog. Soc.* 137, 553-597.
- DHI, 2011. MIKE 21 SW, User manual, DHI Water and Environment, Denmark.
- Dora, G.U., Sanil Kumar, V., 2015. Sea state observation in island-sheltered nearshore zone based on in situ intermediate-water wave measurements and NCEP/CFSR wind data. *Ocean Dynamics* 65, 647-663, doi:10.1007/s10236-015-0822-1.
- Eldeberky, Y., 1996. Nonlinear transformations of wave spectra in the nearshore zone. (Ph.D. thesis). Delft University of Technology, Delft, Netherlands.
- Glejin, J., Sanil Kumar, V., Balakrishnan Nair, T.M., and Singh, J., 2013. Influence of winds on temporally varying short and long period gravity waves in the near shore regions of the eastern Arabian Sea. *Ocean Science* 9, 343–353. doi:10.5194/os-9-343-2013.
- Goswami, B.N., Guoxiong, Wu., Yasunari, T., 2010. The Annual Cycle, Intraseasonal Oscillations, and Roadblock to Seasonal Predictability of the Asian Summer Monsoon. *J. Climate* 19, 20, 5078-5099.
- Harikumar, R., Balakrishnan Nair, T.M., Bhat, G.S., Nayak, S., Reddem, V.S., Sheno, S. S.C., 2013. Ship-Mounted Real-Time Surface Observational System on board Indian Vessels for Validation and Refinement of Model Forcing Fields. *J. Atmospheric and Oceanic Technology* 30, 626- 637.
- Hasselmann, K., Barnett, T.P., Bouws, E., Carlson, H., Cartwright, D.E., Enke, K., Ewing, J.A., Gienapp, H., Hasselmann, D.E., Kruseman, P., Meerburg, A., Müller, P., Olbers, D.J., Richter, K., Sell, W., Walden, H., 1973. Measurements of wind-wave growth and swell decay during the Joint North Sea Wave Project (JONSWAP). *Deutsche Hydrographische Zeitschrift Supplement A*, 8(12) .
- Holthuijsen, L.H., Booij, N., Bertotti, L., 1996. The Propagation of Wind Errors Through Ocean Wave Hindcasts. *J. Offshore Mechanics and Artic Engg.* 118(3), 184-189.
- ITT, 2014. Indian tide tables, Indian and selected Foreign Ports. Survey of India, Government of India. New Delhi, pp. 238.
- Ji, M., Smith, T.M., 1995. Ocean model response to temperature data assimilation and varying surface wind stress. Intercomparisons and implications for climate forecast. *Mon. Wea. Rev.* 123, 1811-1821.
- Kelly, K.A., Dickinson, S., Yu, Z.J., 1999. NSCAT tropical wind stress maps: Implications for improving ocean modeling. *J. Geophys. Res.* 104 (C5), 11 291-11 310.
- Kumar, R., et al., 2000. Ocean wave model sensitivity experiments; Preprints, Fifth Pacific Ocean remote sensing Conf. (PORSEC), Goa, India, 801–803.
- Kumar, P.B., Vialard, J., Lengaigne, M., Murty, V.S.N., McPhaden, M.J., 2012. TropFlux: Air-sea fluxes for the global tropical oceans-Description and evaluation. *Climate Dyn.* 38, 1521-1543, doi:10.1007/s00382-011-1115-0.
- Komen, G., Hasselmann, S., Hasselmann, K., 1984. On the existence of a fully developed wind-sea spectrum. *J. Phys. Oceanogr.* 14(8), 1271–1285.
- Moeini, M.H., Etemad-Shahidi, A., Chegini, V., 2010. Wave modelling and extreme value analysis off the northern coast of the Persian Gulf. *Applied Ocean Res.* 32(2), 209-218.
- Moeini, M.H., Etemad-Shahidi, A., Chegini, V., Rahmani, I., 2012. Wave data assimilation using a hybrid approach in the Persian Gulf. *Ocean Dynamics* 62(5), 785-797.
- Nayak, S., Bhaskaran, P.K., Venkatesan, R., Dasgupta, S., 2013. Modulation of local wind waves at Kalpakkam from remote forcing effects of Southern Ocean swells. *Ocean Engg.* 64, 23-35.

- Neetu, S., Shetye, S. R., Chandramohan, P., 2006. Impact of seabreeze on wind-seas off Goa, west coast of India. *J. Earth Syst. Sci.* 115, 229–234,
- Premkumar, K., Ravichandran, M., Kalsi, S.R., Sengupta, D., Gadgil, S., 2000. First results from a new observational system over the Indian Seas. *Curr. Sci. India* 78, 323-330.
- Putman, W.M., Legler, D. M., O'Brien, J. J., 2000. Interannual variability of synthesized FSU and NCEP reanalysis pseudostress products over the Pacific Ocean. *J. Climate* 13, 3003- 3016.
- Remya, P.G., Raj Kumar, Sujit Basu, Abhijit Sarkar, 2012. Wave hindcast experiments in the Indian Ocean using MIKE 21 SW model. *J. Earth Syst. Sci.* 121, No. 2, 385–392.
- Ris, R.C., Holthuijsen, L.H., Booij, N., 1999. A third-generation wave model for coastal regions 2. Verification. *Journal of Geophysical Res.* 104 (4), 7667-7681.
- Roland, B.S., 1988. An introduction to Boundary Layer Meteorology, Kluwer Academic Publishers, 666 pp.
- Samiksha, S.V., Polnikov, V.G., Vethamony, P., Rashmi, R., Pogarskii, F., Sudheesh, K., 2015. Verification of model wave heights with long-term moored buoy data: Application to wave field over the Indian Ocean, *Ocean Engg.* 104, 469–479.
- Sandhya, K.G., Balakrishnan Nair, T.M., Bhaskaran, P.K., Sabique, L., Arun, N., Jeykumar, K., 2014. Wave forecasting system for operational use and its validation at coastal Puducherry, east coast of India. *Ocean Engg.* 80, 64-72. doi: 10.1016/j.oceaneng.2014.01.009.
- Sanil Kumar, V., Anand, N.M., Kumar, K.A., Mandal, S., 2003. Multi peakedness and groupiness of shallow water waves along Indian coast, *J. Coastal Res.* 19(4), 1052-1065.
- Sanil Kumar, V., Shanass, P.R., Dubhashi, K.K., 2014. Shallow water wave spectral characteristics along the eastern Arabian Sea. *Natural Hazards* 70, 377–394, doi:10.1007/s11069-013-0815-7.
- Sanil Kumar, V., Glejin, J., Dora, G.U., Sajiv, P.C., Singh, J., Pednekar, P., 2012. Variations in nearshore waves along Karnataka, west coast of India. *J. Earth Syst. Sci.* 121, 393-403. doi: 10.1007/s12040-012-0160-3.
- Shanass, P.R., Sanil Kumar, V., 2014. Temporal variations in the wind and wave climate at a location in the eastern Arabian Sea based on ERA-Interim reanalysis data. *Natural Hazards and Earth System Sciences* 14, 1371–1381, doi:10.5194/nhess-14-1371-2014.
- Shukla, J., 1975. Effect of Arabian Sea-surface temperature anomaly on Indian summer monsoon: A numerical experiment with the GFDL model. *J. Atmospheric Science* 32, 503–511.
- Strauss, D., Mirferendesk, H., Tomlinson, R., 2007. Comparison of two wave models for Gold Coast, Australia. *J. Coastal Research*, SI 50 (Proceedings of the 9th International Coastal Symposium), 312 – 316.
- Tolman, H.L., 1989. The Numerical Model WAVEWATCH: A Third Generation Model for the Hindcasting of Wind Waves on Tides in Shelf Seas. *Communications on Hydraulic and Geotechnical Engineering*, Delft University of Technology. ISSN 0169-6548. Report no. 89-2,72.
- Tolman, H.L., 1991. A third-generation model for wind waves on slowly varying, unsteady and inhomogeneous depths and currents. *J. Phys. Oceanogr.* 21, 782–797.
- Tolman, H.L., 2008. A mosaic approach to wind wave modeling. *OceanModelling* 25, 35–47.
- WAMDI Group, 1988. The WAM Model-A third generation ocean wave prediction model. *J. Phys. Oceanogr.* 18, 1175-1810.

Table 1. Statistics for significant wave height and mean wave period from the wave model WW3 using ST4 physics compared to measurements from the buoy at deep water location during July-December 2009

Statistics	Significant wave height, H_s (m)	Mean wave period, T_{m01} (s)
BIAS	-0.19	0.61
Correlation coefficient	0.97	0.59
RMSE	0.38	1.47
SI	0.16	0.17

Table 2. Statistics for significant wave height based on different whitecapping formulation in SWAN compared to measurements from buoy in nearshore

Formulation	BIAS (m)	Correlation coefficient	RMSE (m)	SI
Komen	0.08	0.92	0.29	0.16
Westhuysen	-0.35	0.90	0.48	0.26
Janssen	0.17	0.91	0.34	0.18

Table 3. Statistics for significant wave height, mean wave period, peak wave period and mean wave direction from SWAN nested with WW3 using ST2 and ST4 physics and measured data in different seasons off Karwar during 2014

Statistical parameter	season	ST2 physics in WW3				ST4 physics in WW3			
		H_s (m)	T_{m02} (s)	T_p (s)	Dir (deg)	H_s (m)	T_{m02} (s)	T_p (s)	Dir (deg)
<i>BIAS</i>	Pre-monsoon	0.03	-0.86	-0.20	14.23	-0.07	-1.62	-0.06	15.16
	Monsoon	0.03	1.14	-0.31	3.31	0.02	1.04	-0.73	3.47
	Post-monsoon	0.10	-0.84	0.88	3.83	-0.01	-1.59	0.20	6.63
	Full year	0.05	-0.18	0.13	6.98	-0.02	-0.71	-0.20	8.29
Correlation coefficient (<i>r</i>)	Pre-monsoon	0.65	0.42	0.35	0.57	0.70	0.33	0.46	0.59
	Monsoon	0.92	0.66	0.55	0.60	0.92	0.58	0.60	0.59
	Post-monsoon	0.78	0.53	0.10	0.56	0.83	0.53	0.53	0.53
	Full year	0.96	0.67	0.29	0.56	0.96	0.64	0.52	0.55
<i>RMSE</i>	Pre-monsoon	0.14	1.35	3.85	31.23	0.15	1.87	3.60	31.28
	Monsoon	0.28	1.38	2.32	13.73	0.27	1.42	2.25	13.84
	Post-monsoon	0.17	1.36	4.58	25.26	0.12	1.90	2.98	26.75
	Full year	0.21	1.36	3.71	24.36	0.19	1.74	2.99	24.94
<i>SI</i>	Pre-monsoon	0.19	0.28	0.31	0.13	0.20	0.38	0.29	0.13
	Monsoon	0.15	0.23	0.20	0.06	0.14	0.23	0.19	0.06
	Post-monsoon	0.28	0.28	0.38	0.11	0.20	0.38	0.25	0.11
	Full year	0.19	0.26	0.31	0.10	0.18	0.33	0.25	0.10

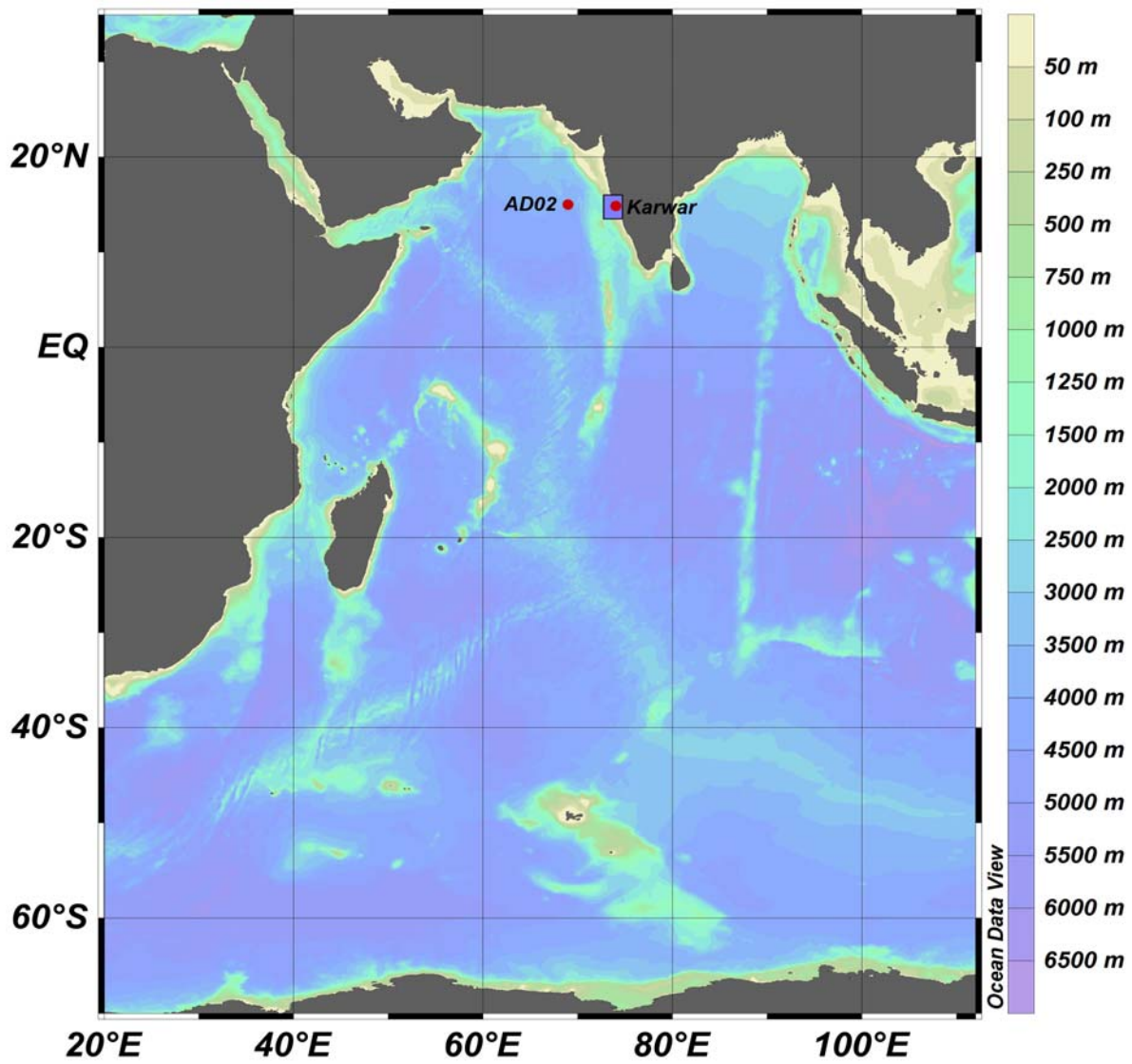


Figure 1. Locations of wave measurements (AD02 and Karwar) and model domain for WW3. The small rectangle around Karwar shows the model domain for SWAN.

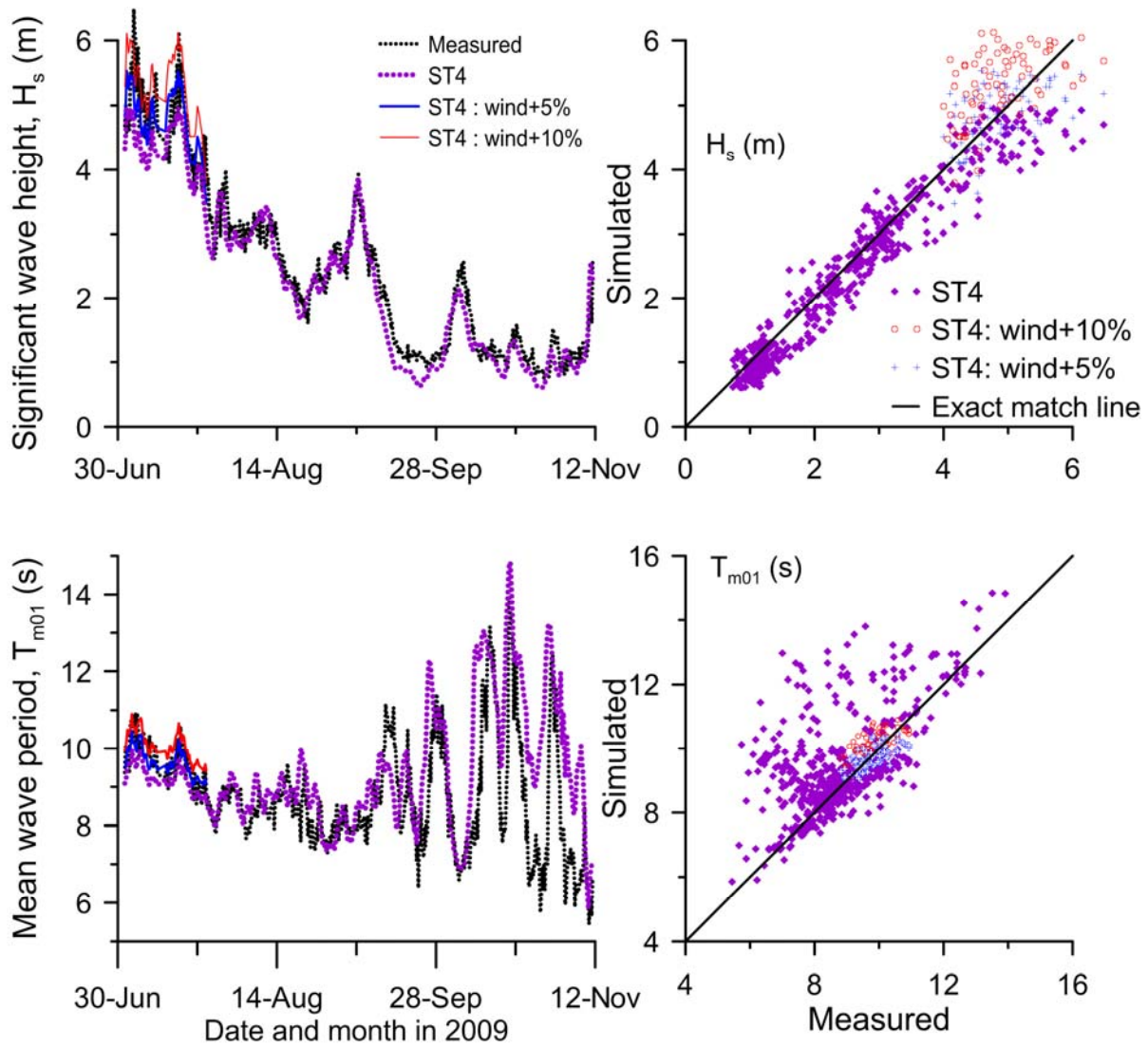


Figure 2. Comparison of measured and simulated significant wave height (H_s) and mean wave period (T_{m01}) from WW3 at a deep water point (left side) during 2009 and the scatter plot for the same (right side). The simulated data with modified forcing fields is also plotted for July. The ST4 physics is used for this simulation. The simulated wave parameters with wind correction for high waves ($H_s > 4$ m) are also presented.

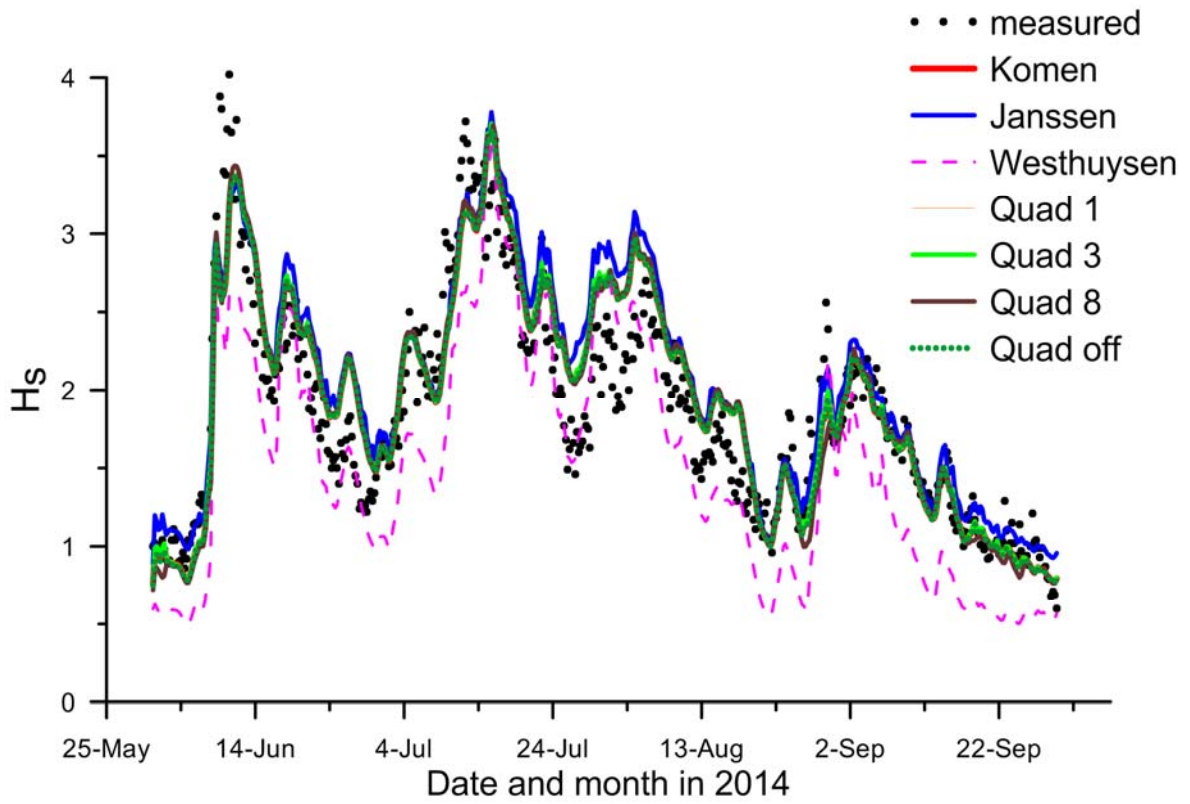


Figure 3. Comparison of measured significant wave height with that estimated using different formulations in SWAN

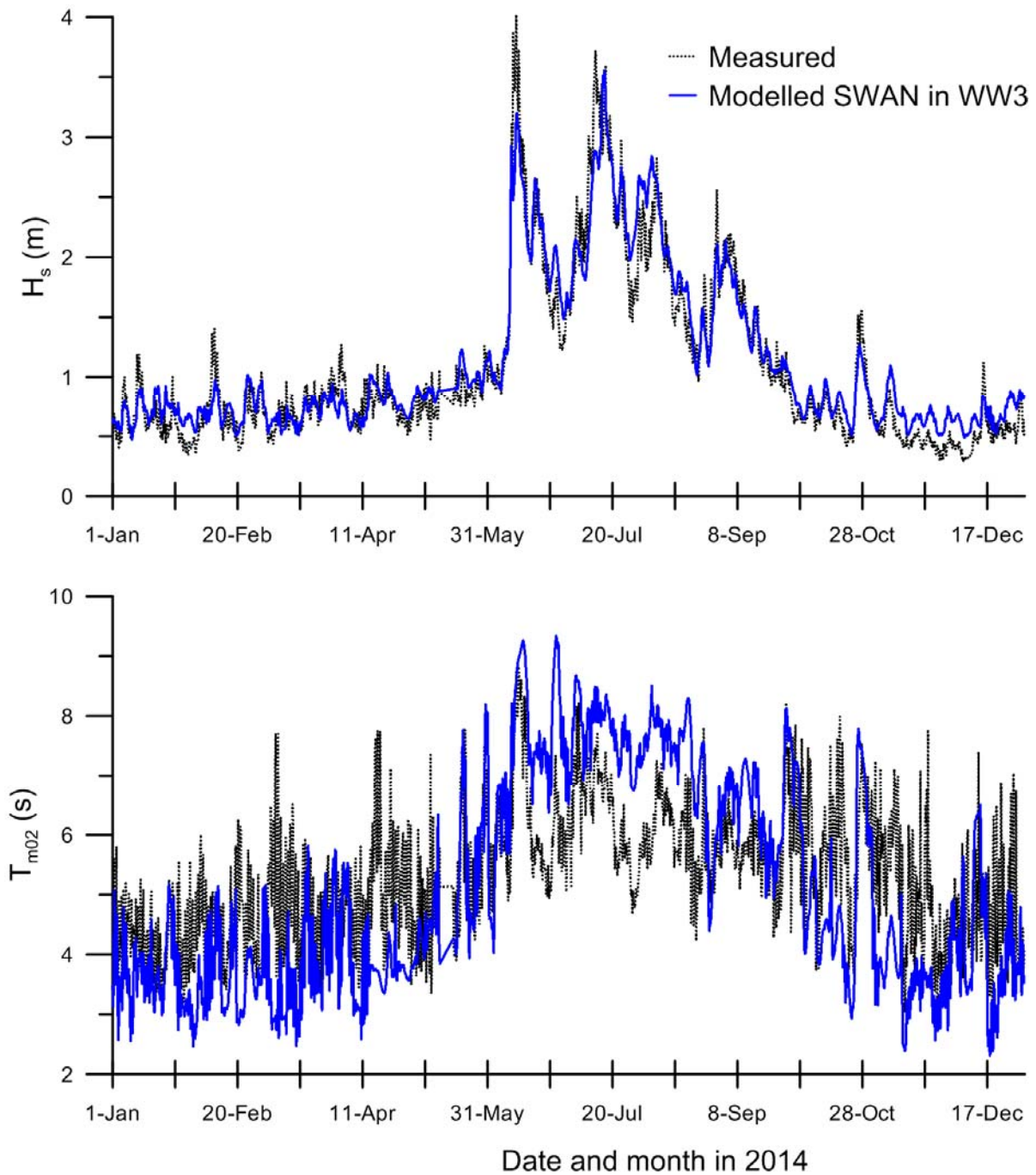


Figure 4. Comparison between measured and simulated wave parameters; significant wave height and mean wave period in nearshore waters of Karwar using SWAN nested with WW3 using ST2 physics

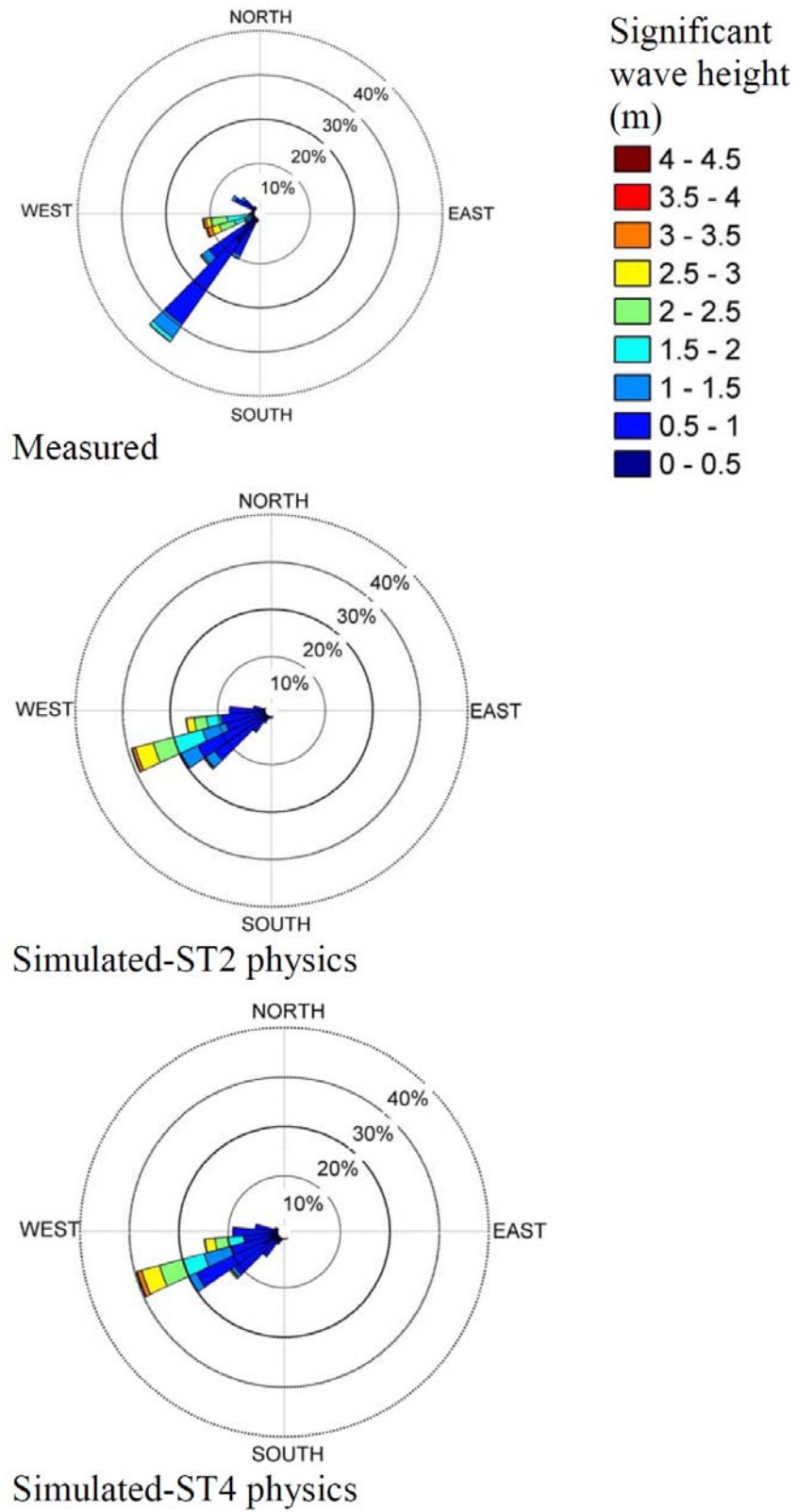


Figure 5. Comparison between measured and simulated wave direction in nearshore waters of Karwar using SWAN nested with WW3 using ST2 and ST4 physics

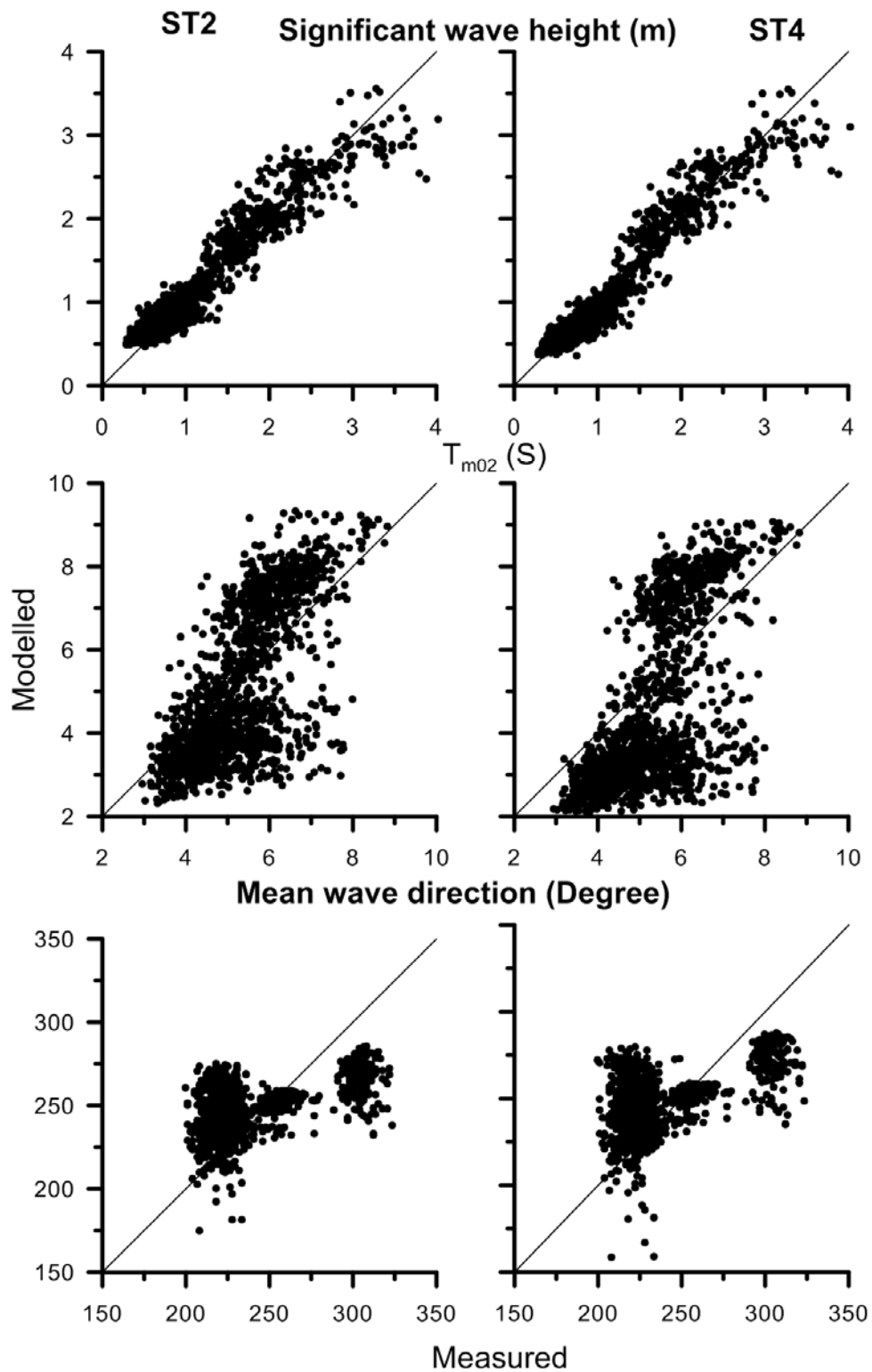


Figure 6. Scatter plot of measured and modelled wave parameters in nearshore waters of Karwar; a) significant wave height, b) mean wave period and c) mean wave direction for the year 2014. Left panel is based on ST2 physics and right panel is based on ST4 physics in WW3

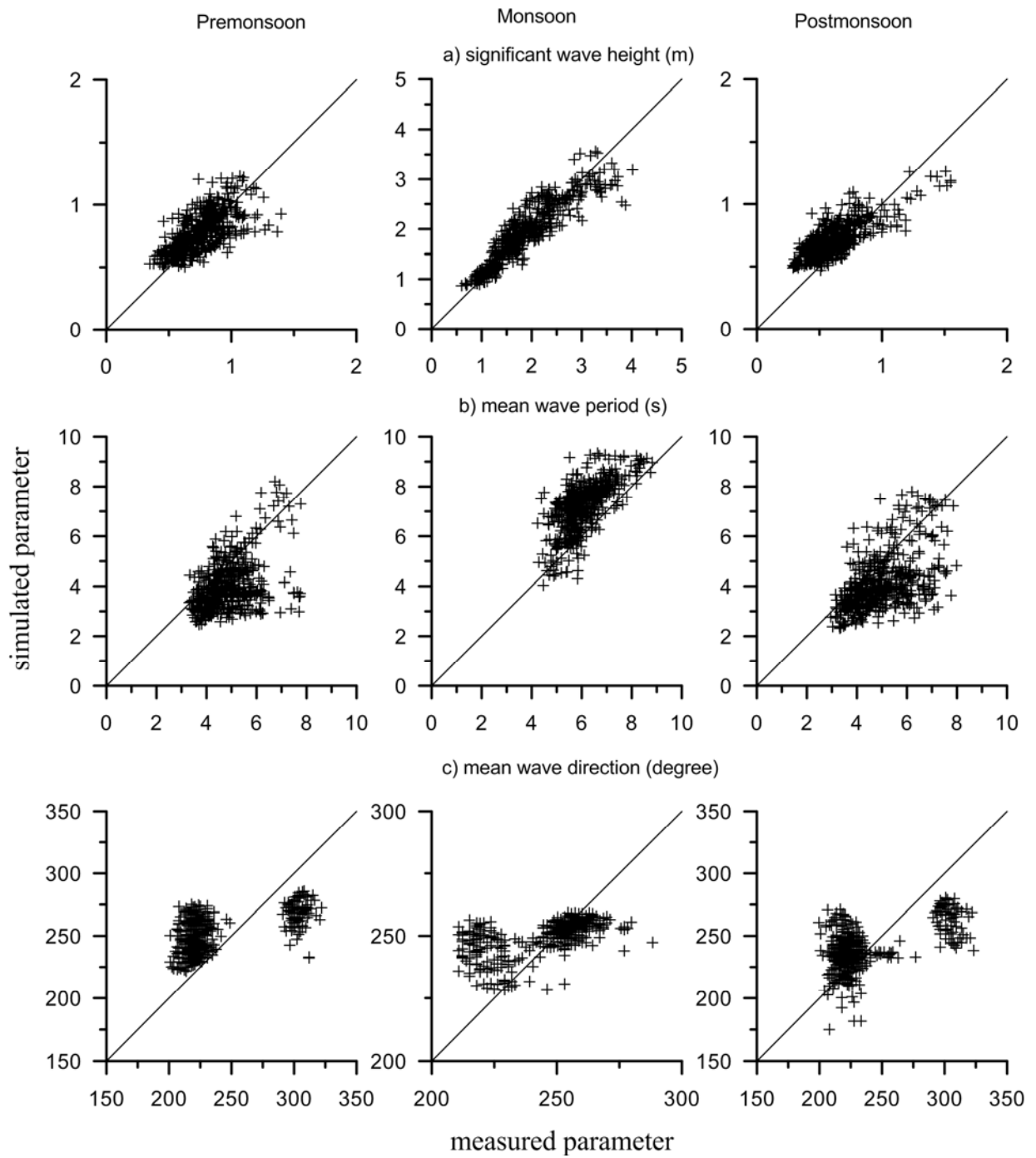


Figure 7. Scatter plot of measured and hindcasted wave parameters for different seasons based on ST2 physics in WW3

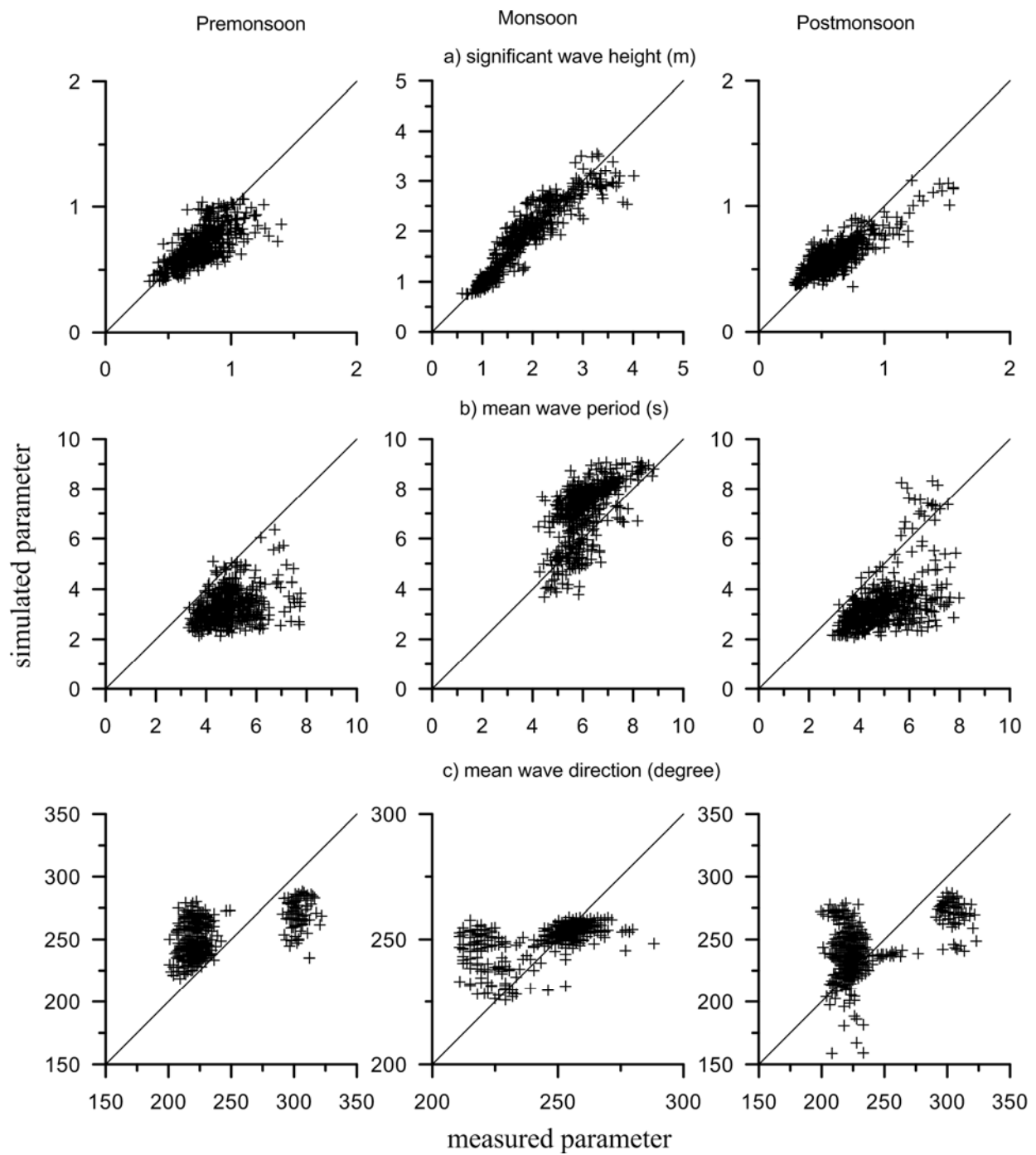


Figure 8. Scatter plot of measured and hindcasted wave parameters for different seasons based on ST4 physics in WW3

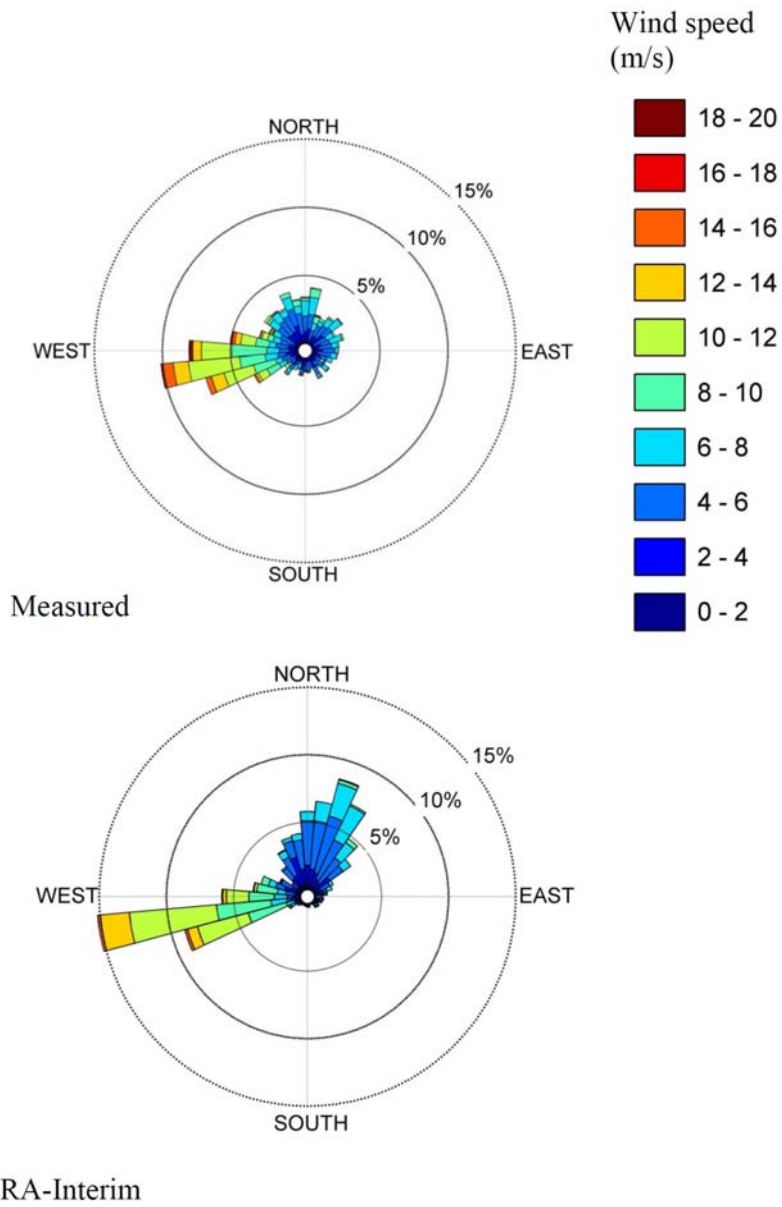


Figure 9. Wind rose diagram comparing the measured and ERA-Interim wind speed at the deep water point 15.0000°N, 69.0000°E